Title
PHOTOELECTRON SPECTROSCOPY: A CHEMICAL TOOL FROM NUCLEAR SPECTROSCOPY

Permalink
https://escholarship.org/uc/item/74p6z6cv

Authors
Hollander, Jack M.
Hollander, Jack M.

Publication Date
1969-08-01

Presented at Intern. Conf. on Radioactivity
in Nuclear Spectroscopy, Nashville, Tennessee,
August 11-15, 1969

UCRL-18972
Preprint

cy. 2

PHOTOELECTRON SPECTROSCOPY: A CHEMICAL TOOL FROM NUCLEAR SPECTROSCOPY

Jack M. Hollander

August 1969

AEC Contract No. W-7405-eng-48

LAWRENCE RADIATION LABORATORY
UNIVERSITY of CALIFORNIA BERKELEY

cy. 2

UCRL-18972

DISCLAIMER

PHOTOELECTRON SPECTROSCOPY:
A Chemical Tool from Nuclear Spectroscopy*

Jack M. Hollander

Lawrence Radiation Laboratory
University of California
Berkeley, California 94720

August 1969

INTRODUCTION

Throughout the history of nuclear spectroscopy, the interaction between chemistry and physics, and between chemists and physicists, has been strong. The contribution of nuclear chemists, for example, to the techniques of source purification and preparation was indispensible to the successful study of the spectroscopy of rare-earth and actinide nuclei. And had it not been for the nuclear chemists, there would have been no actinide nuclei to study.

But the flow of benefits has not been unidirectional. The field of chemistry has itself benefited in many ways from nuclear spectroscopy. To appreciate the recent impact of nuclear spectroscopy on chemistry, one has only to note the tremendous advances that have taken place in activation analysis as a result of the semiconductor detector revolution.

Another advance in chemistry that has arisen out of nuclear spectroscopy, is the technique of photoelectron spectroscopy. This review will trace the development of this new spectroscopy and will illustrate some of the applications that have attracted interest among chemists. Photoelectron spectroscopy deals with the chemist's "forgotten electrons", those in the atomic core, which in recent years have played only a minor role in chemistry. To the chemist the K shell is virtually as remote as the nucleus, contributing neither to chemical bonding nor being affected appreciably by chemical bonding, remaining instead characteristic of the atom.

The photoelectron effect involving the inner shells has of course long been known, since it is one of the fundamental modes of photon absorption in matter, but beyond early efforts to verify the theory of the photoelectric effect little use was made of inner-shell photoemission to study physical or chemical phenomena.

The inner atomic levels have on the other hand played a prominent role in nuclear spectroscopy, in the study of internal conversion and orbital electron capture. In the early 1950's, as great advances in nuclear spectroscopy were taking place, magnetic analysis of internal conversion spectra became a precise technique for the study of nuclear levels, and the determination of internal conversion coefficients became increasingly important in ascertaining transition properties and level quantum numbers. The need to have a high resolution method for the determination of internal conversion coefficients led Hultberg and his associations in Stockholm to explore the use of photoelectron spectroscopy ("external conversion") for precise measurement of gamma-ray intensities, with use of the magnetic spectrometers developed for internal conversion studies. In the course of these studies, much new information was gained about photo cross-sections and about the angular distributions of photoelectrons.

During the same period it became apparent that the numerical values of the atomic electron binding energy, a quantity that enters into the calculation of the nuclear transition energy from internal conversion or photoelectron data, were not known to sufficient accuracy. Experimental errors in the determination of energy levels were being reduced to the neighborhood of 10 eV, less than the uncertainties in many cases of the atomic electron binding energies. In order to reduce these uncertainties, K. Siegbahn and his associates in Uppsala began a systematic study of electron binding energies of all the elements, with use of a new high-resolution iron-free magnetic spectrometer. The technique employed was to irradiate solid targets with x-rays and measure the kinetic energies of the ejected photoelectrons. The first measurements were done with molybdenum and copper x-rays, and photoelectron line widths as small as 5 eV were obtained. Refinements of technique, including the use of lower atomic number x-ray sources and improved electron detectors, have subsequently brought the line-widths down to 1 eV or even lower.

The interaction of photoelectron spectroscopy with chemistry began with the discovery by the Uppsala group that peak shifts in the K-shell photolines were taking place in different compounds of the same element. As the result of extensive studies of these binding energy shifts in many different chemical systems, photoelectron spectroscopy has developed into a research tool of wide applicability in chemistry, solid-state physics, and biology. A detailed description of the method is given in the book ESCA, Atomic, Molecular, and Solid State Structure Studied by Means of Electron Spectroscopy, by Siegbahn *et al*.[1]

EXPERIMENTAL TECHNIQUE

The experimental technique of photoelectron spectroscopy is illustrated in Fig. 1. Solid or gaseous samples are exposed to a flux of x-rays of known energy, and the photoelectrons expelled by these x-rays are energy analyzed in the spectrometer. Most commonly the Mg K_α line (unresolved K_{α_I} and $K_{\alpha_{II}}$) is used as the x-ray source. This line has an energy of 1253.6 eV and a natural width of about 0.5 eV. Additional contributions to the line width from spectrometer focusing aberrations, atomic level width, and solid effects bring the total observed line widths (FWHM) for solids to 1.3-1.6 eV. For gases the lines are narrower, 0.8-1.2 eV.

Figure 2 shows a comparison of two sets of data involving the L_{II} and L_{III} levels of copper ($2p_{1/2}$ and $2p_{3/2}$), from Siegbahn et al.[1] The upper spectrum was obtained with use of a high-resolution x-ray spectrometer and the lower one is a photoelectron spectrum taken with Mg K_{α} radiation. The considerably narrower width of the photo lines is evident. The reason for the difference is that the Cu K level is involved in the x-ray transition, but the narrower Mg K level is involved in the photo-line.

Figure 3 shows a comparison between a photoelectron spectrum and an x-ray absorption spectrum in the vicinity of the K-edge.[1] This is of interest because of the fact that chemists had long noted chemical effects on the shapes of absorption edges but had found them difficult to interpret. The figure illustrates the problem; near an absorption edge the electron being ejected by the x-ray does not go into the continuum but rather into a final state that might be, for example, a band of closely spaced unoccupied levels in the conduction band whose nature and spacing depend on specific properties of the solid. With x-ray photoelectron spectroscopy, on the other hand, the electron is sent far enough into the continuum so that there is no appreciable structure in the final state.

To the nuclear spectroscopist who has worked with low-energy electrons in the range of 10 to 50 keV and has experienced the difficulties of preparing thin sources for high-resolution electron spectroscopy, the narrowness of the photoelectron lines may seem surprising. Interestingly, however, high-resolution electron spectroscopy at 1 keV becomes easier than at 20 keV. The reason for this is related to the smaller absolute width of a 1 keV line as compared with a 20 keV line (for equivalent resolution). Energy losses of electrons traversing a solid are discrete, and the most probable energy-loss quanta are much larger than 1 eV. Thus in the case of the low-energy line, having a width of about 1 eV, most of the electrons that have sustained losses are thrown well outside the peak. On the other hand with the higher energy lines encountered in internal conversion, the energy losses are comparable in magnitude to the line width ($\geqslant$20 eV for a 20 keV line) so that the energy-loss electrons form a low-energy "tail" or broadening of the line. This is not to imply that line broadening due to solid effects does not occur at all in photoelectron spectroscopy; small effects such as plasmon oscillations are seen that cause the lines from solids to be several tenths of eV wider than the lines from gases.

The binding energy of a particular atomic shell is determined experimentally by subtracting the measured electron kinetic energy of the corresponding photoelectron line from the energy of the exciting photon (Mg K_α), which is accurately known. In work with gases, the binding energy is referenced to the vacuum level. In solids it is more convenient to use the Fermi level as the reference so that the work function of the solid need not be determined. (There is a correction for the work function of the spectrometer material, but it is a constant for all measurements and does not enter the calculation of chemical shifts). An energy conservation diagram for the process is shown in Fig. 4.

Figure 5 is another illustrative photoelectron spectrum, showing the outer levels in platinum.[2] This figure demonstrates that the outer levels of the atom can be seen with complete resolution of the N_{VI} and N_{VII} spin doublet ($4f_{5/2}$ and $4f_{7/2}$). Note also the satellite lines from the $K_{\alpha_{3,4}}$ x-ray group. The conduction band is also seen clearly. The O_{III} ($5p_{3/2}$) line has proven to be quite interesting, and it will be discussed further below.

APPLICATIONS OF PHOTOELECTRON SPECTROSCOPY

The power of the photoelectron method comes from the fact that the observable quantity, the electron binding energy, is directly related to the Coulomb and exchange interactions within the atom being studied, that is, to the effective charge on the atom. Thus changes or shifts in binding energy in a series of compounds should relate to the differences in charge or other features of chemical structure.

The origin and approximate magnitude of the chemical shift in core electron binding energies is demonstrated by a simple charged shell model. If the valence orbitals of an atom are considered as a charged spherical shell of radius r, then removal of electronic charge q from the valence shell to infinity will cause a change in the potential energy inside the sphere, ΔE, given in atomic units by the relation $\Delta E = q/r - q/\infty$. With a charged shell mean radius of 1 Å, $\Delta E \approx 14$ eV if $q = 1$. All the core electrons inside the sphere are, therefore, increased in energy by the amount ΔE. Shifts from actual chemical bond formation are expected to be less than this ΔE, both because fewer than one charge is transferred in most chemical changes and also because electrons are not usually transferred to infinity. For a simple ionic bond, one can represent the change in potential as $q/r - q/R$, where R is the nearest-neighbor distance, to which the charge is transferred when the ionic bond is formed. In covalent bonding the charge transfer is much less, but the charged shell model can be used to describe this case also in terms of the smaller distance through which the charge is transferred.

The following are some illustrative examples of the application of the photoelectron method in chemistry:

1) Systematics of chemical shifts in molecular systems.

One of the important applications of photoelectron spectroscopy is in the area of molecular structure. Electron binding energies of an atom correlate with the oxidation state of the atom--the higher the oxidation state or effective charge on the atom, the higher the binding energy. This correlation is intuitively sound because one expects an electron to be held more tightly to a positively charged atom than to a negatively charged atom.

A good example of the chemical-structure dependence of binding energy is seen in the spectrum of the carbon 1s level in ethyl trifluoro-acetate, Fig. 6, recorded by Siegbahn and co-workers in Uppsala.[1] Here there are four carbon atoms with distinctive character owing to their place in the molecule, and four resolved lines appear in the spectrum. The carbon of the CF_3 group is the most positive since the electronegativity of fluorine is very high; the carbon of the CH_3 group is the least positive. This simple electronegativity picture is sufficient to explain the trend in the experimental binding energies, since the CF_3 carbon has the highest binding energy, the C=O carbon the next, the $O-CH_2$ carbon the next, and the CH_3 carbon the lowest binding energy. This large shift in the carbon 1s level in different environments suggests that many interesting studies of carbon-containing molecules will be possible.

In a chemical reaction, the amount of binding energy shift is an indication of the charge transfer in the reaction. It is interesting how different these shifts can be, per unit oxidation number change. For example, in iodine the average shift in going from the -1 to the +7 state is 0.8 eV per oxidation number, but in europium a shift of 9.6 eV is seen from Eu^{+2} to Eu^{+3}.[3] This indicates that much more charge is transferred in the europium oxidation. In that case it is a good approximation to say that one 4f electron is transferred in going from the +2 to the +3 state, whereas in the case of iodine fewer than one charge is transferred per unit oxidation number change.

Attempts were made to correlate the earliest observed chemical shifts with valence or formal oxidation number of an element in different compounds. Since oxidation number is only a formal concept in which the electrons are assigned to one atom or another, these correlations were not very good. A closer approach to reality was to correlate shifts with atom charges estimated by means of the simple Pauling valence-bond model, a semi-empirical method in which charge is assigned to the various atoms on the basis of their electronegativities and of the bond-lengths involved.[1] These correlations are much better than those using simple valence numbers. Most recently, sophisticated molecular orbital methods have been used for estimating atomic charges. Figure 7 shows a correlation of binding energy data for nitrogen 1s electrons with atom charges calculated with the CNDO (Pople) and Extended-Hückel methods, by Hendrickson et al.[4] These correlations are better, though not strikingly so, than those made with simple Pauling estimates of charge.

Correlations of this kind are useful in several ways. They are an aid in inferring structural information about new compounds or complicated compounds for which the molecular orbital calculations are not feasible. Also, the quality of the correlation tells something about the validity of the theoretical methods used for estimating charge. There are however at least two deficiencies in the use of atomic charge-binding energy correlations. First, the fits are not terribly good, and the large amount of scatter (see Fig. 7) suggests that there is not an exact one-to-one correspondence between binding energy and atomic charge. Second, the available methods for calculating atomic charges yield quite different values of the charges, so that one cannot attach quantitative significance to the absolute values of the charges; it is therefore difficult to infer chemical information from the "experimental" values of charge found from measurement of binding energies.

It would be desirable to relate measured binding energies to some quantity that has definite chemical significance, or better still, that can be measured. Hendrickson and Jolly[5] have worked out a thermochemical cycle, including the photoelectron emission process, in which only experimentally measurable quantities enter. This cycle is established with use of a concept called "equivalent cores", which says that cores having the same charge are chemically equivalent.

Consider the following cycle of reactions, the sum of which represents the photoelectron emission from a typical solid compound, $NaNO_2$.

$$NO_2^- \text{ (lattice)} \longrightarrow NO_2^- \text{ (gas)} \qquad (1)$$

$$NO_2^- \text{ (gas)} \longrightarrow NO_2^* \text{ (gas)} + e^- \text{ (gas)} \qquad {}^* = \text{K hole} \qquad (2)$$

$$NO_2^* \text{ (gas)} \longrightarrow NO_2^* \text{ (lattice)} \qquad (3)$$

$$e^- \text{ (gas)} \longrightarrow e^- \text{ (Fermi)} \qquad (4)$$

$$NO_2^- \text{ (lattice)} \longrightarrow NO_2^* \text{ (lattice)} + e^- \text{ (Fermi)} \qquad (5)$$

These reactions and the energies involved in them are considered as follows: Process (1) consists in the removal of the ion NO_2^- from its site in the crystal lattice. If the ion is removed from the bulk material (rather than from the surface) the energy of this process is by definition equal to the lattice energy of the crystal, and the equation may be rewritten thus:

$$NaNO_2 \text{ (lattice)} \longrightarrow Na^+ \text{ (gas)} + NO_2^- \text{ (gas)} \quad . \qquad (6)$$

In Process (2) a core electron is removed from the nitrogen atom in the gaseous species NO_2^-. Consider the nitrogen atom in the resultant species NO_2^*, which has a missing 1s electron. According to the concept of equivalent cores, to its valence electrons this nitrogen atom looks just like the central oxygen atom in an O_3 molecule. (The oxygen atom actually has one more nuclear charge and one more core electron, but the assumption is that this difference is not "noticed" by the valence electrons during the time of photoelectric event.) Thus one can write the following chemical equation which involves no energy change (within the limits of the approximation):

$$NO_2^* \text{ (gas)} + O^+ \text{ (gas)} \longrightarrow O_3 \text{ (gas)} + N^{+*} \text{ (gas)} \quad . \qquad (7)$$

Note that this equation is completely balanced, including numbers of atoms, charge, and K-holes. Addition of reactions (7) and (2) gives:

$$NO_2^- \text{ (gas)} + O^+ \text{ (gas)} \longrightarrow O_3 \text{ (gas)} + N^{+*} \text{ (gas)} + e^- \text{ (gas)} \quad . \qquad (8)$$

With use again of the "equivalent core" assumption, process (3) is rewritten as the condensation of gaseous O_3 into a hole in a lattice of solid O_3, that is:

$$2O_3 \text{ (gas)} \longrightarrow 2O_3 \text{ (lattice)} \quad . \qquad (9)$$

By adding equations (6), (8), and (9) which correspond to processes (1), (2), and (3), the following overall equation is obtained:

$$\begin{aligned} NaNO_2 \text{ (lattice)} + O^+ \text{ (gas)} + O_3 \text{ (gas)} &\longrightarrow Na^+ \text{ (gas)} \\ &+ 2O_3 \text{ (lattice)} + N^{+*} \text{ (gas)} + e^- \text{ (gas)} \quad . \end{aligned} \qquad (10)$$

The energy change involved in this reaction can in principle be evaluated from chemical thermodynamic data (heats of formation). In a <u>series</u> of nitrogen compounds, the species O^+ (gas) and N^{+*} (gas) always enter the corresponding equations in the same way; thus their heats of formation can be ignored as they will cancel in taking <u>differences</u> in the reaction energies. The same is approximately true for the work function correction (process (4)).

Equations similar to (10) can be written for other nitrogen compounds whose x-ray photoelectron spectra have been obtained, and some of them are given in Fig. 8. From the binding-energy data obtained by Hendrickson *et al.*[4] from a series of nitrogen compounds, the thermochemical energies and the corresponding experimental *1s* binding energies are plotted in Fig. 9. The binding energy is seen to be a linear function of the thermochemical energy evaluated in this way, and the scatter of points is considerably less than found in plots of binding energy versus estimated atomic charge. These results establish the utility of the equivalent core approximation, and with this method predictions of heats of formation can be made in many cases for unknown species. It should be mentioned that the major component of the equivalent-core approximation is actually the assumption that the x-ray photoelectric transition takes place in a time interval short compared with the lifetime of the core-electron hole. This is a plausible assumption since the photoelectric process is believed to occur in around 10^{-18} sec whereas the lifetime of a K-hole is around 10^{-16} sec.[6]

2) Structure of the Oxyhyponitrite ion, $N_2O_3^{--}$.

An interesting example of the use of photoelectron spectroscopy in structural chemistry is the proof of the existence of structurally different nitrogen atoms in the $N_2O_3^{--}$ ion. The three possible structures previously proposed for this ion are shown in Fig. 10. The earlier measurements, involving calorimetry, ultra-violet and infra-red spectroscopy, had been mutually inconsistent.

In structure I, the two nitrogens are chemically equivalent. This structure was unequivocally ruled out by the photoelectron measurements, which reveal two distinct nitrogen 1s lines (Fig. 11). Molecular orbital calculations made with structures II and III indicated that in III the nitrogen charges are almost equal. Only structure II is consistent with the observed binding energy difference between the two nitrogens, and the charges calculated for this structure fit very well on the correlation diagram (Fig. 7).[4]

3) Character of metal-coordinated ligands.

The power of the method is illustrated by Fig. 12, which shows the nitrogen 1s spectrum from trans $[Co(NH_2\ CH_2\ CH_2\ NH_2)_2(NO_2)_2]NO_3$. Here the different charges on the nitrogen atoms in the several ligands (groups) are clearly in evidence.[4]

By photoelectron spectroscopy it was also possible to show[4] that the ammonia (NH_3) group as coordinated to metals such as CoIII, RhIII, IrIII, and CrIII exhibits some ammonium-like (NH_4^+) character. This result is based on the observation that the nitrogen 1s binding energy in these complexes is intermediate between that in free NH_3 and in NH_4NO_3 (NH_4^+ nitrogen).

4) Character of NO group in metal nitrosyls.

Two examples of metal nitrosyls are:

$$\text{FeII:}\ [Fe(\underset{\overset{\uparrow}{398.2}}{CN})_5\underset{\overset{\uparrow}{403.3}}{NO}]^{--} \qquad \text{CrI:}\ [Cr(\underset{\overset{\uparrow}{398.4}}{CN})_5\underset{\overset{\uparrow}{400.7}}{NO}]^{---}$$

The numbers shown are the N 1s binding energies of the corresponding nitrogen atoms, in eV. Note that the change of metal does not affect the CN^- group much, but the NO^+ group is strongly affected, with the NO^+ in the chromium complex being the more negative. This agrees with observations made on these same compounds by infra-red spectroscopy, where the CN stretching frequency is relatively constant but the NO frequency changes from ≈ 1900 to ≈ 1600 cm^{-1}. The explanation for this behavior is in terms of the empty π orbital of the NO^+ which is available for back donation of electrons from the metal. In general, this back-donation is greater in compounds with lower oxidation states. This is consistent with the NO^+ in the chromium compound being the more negative of the two.

5) Crystal-field splitting of core-electron levels.

Some very interesting applications of photoelectron spectroscopy have come about because of the ability of the high-resolution spectra to reveal small splittings of normally degenerate atomic levels and thereby provide a means to study the nature of the interactions that cause the lifting of the degeneracy. Two types of splittings have been observed: quadrupole splitting and exchange splitting. The interaction of nuclear spectroscopy with the newer field is further illustrated by the following example.

5.a) Quadrupole splittings. In the course of high-resolution studies of internal conversion spectra, Novakov and Hollander[7] investigated the effects of placing a radioactive source in a very high electric field. A change in conversion electron line-shape, interpreted at the time as an atomic level splitting, was seen in electron lines from conversion in $p_{3/2}$ levels. The results of this experiment were difficult to interpret however, because of the relatively large line-widths (high kinetic energies) involved.

The same authors later searched for atomic-level splitting by means of photoelectron spectroscopy, and here the complex structure of $p_{3/2}$ photolines was clearly seen.[8] Figure 13 shows some of the results for compounds of uranium and thorium, where structure in the $p_{3/2}$ lines is evident. With various uranium compounds, different splitting energies were measured, ranging from 3 to 10 eV (the latter in uranyl acetate). In one case, where a crystallization was done inside the spectrometer, it was actually possible to follow a change of the level splitting with time.

These splittings were interpreted as arising from internal electric field gradients and their interaction with $p_{3/2}$ electrons, which causes the levels to split into the $M = \pm 1/2$ and $\pm 3/2$ substates.

In an effort to gain more information on this phenomenon, photoelectron spectra from some gold compounds were studied.[9] This was of interest because of the results of a recent study of nuclear quadrupole splitting in gold compounds made by Faltens and Shirley by Mössbauer spectroscopy.[10] The Mössbauer nuclear level quadrupole splitting in linear aurous compounds was explained as being due to the contribution to chemical bonding of the 6p electrons outside the $5d^{10}$ core of Au^+. If the linear X-Au-X unit were completely ionic, the nuclear quadrupole splitting would be zero because of the spherical symmetry of the electron shells in the Au^+ ion. On the other hand, if there is a covalent contribution to bonding from, for example, sp-hybrid orbitals, a field gradient would be produced at the nucleus because of the participation of the 6p orbitals, and quadrupole splitting of nuclear levels could be found. Similarly, the 6p orbitals could produce a gradient at the (filled) 5p orbital, which might be responsible for splitting of the $5p_{3/2}$ atomic level.

Figure 14 shows portions of the photoelectron spectra obtained with Au metal, AuCN, and $KAu(CN)_2$, and Fig. 15 shows how the observed $p_{3/2}$ level splittings correlate with the Mössbauer nuclear quadrupole splittings in the same compounds.[9] Although the curve shown is preliminary the correlation is good and does indicate that the same cause, i.e., the internal electric field gradient, is responsible for the splittings in both situations.

The spectrum of Fig. 13 indicates that thorium metal has a split $p_{3/2}$ line. This observation may seem inconsistent with the explanation offered for the splitting because thorium has a cubic (face centered) structure which should not produce quadrupole fields at the sites of the atoms in the crystal. That the splitting is seen could however be due to gradients existing near the surface because of oxidation, since the near-surface region is known to be the source of most of the observed photoelectrons.

5.b) Exchange splitting. Watson and Freeman[11] have predicted a splitting in core levels of transition group compounds because of the exchange interaction between the spin-up electrons and the unpaired *d* electrons. Quantitative estimates of the splitting energy made by unrestricted Hartree-Fock calculations on free atoms indicate that splittings of up to 10 eV might be found.[11] Fadley and Shirley[12] have searched for this effect in solids by photoelectron spectroscopy and have recently found splittings of 3*s* levels of about 6 eV in MnF_2, MnO, and FeF_3. A portion of one of their spectra is shown in Fig. 16.

Splittings of this origin have also been seen in gaseous molecules by Hedman *et al.*[13] in Uppsala. Their data are shown in Fig. 17. The 1*s* level of the O_2 molecule, which has two unpaired electrons and is paramagnetic, is observed to be split. The N_2 molecule, which is diamagnetic with no unpaired electrons, shows no splitting. Splitting is also observed in the paramagnetic NO molecule. The relative intensities of the lines are explained by Hedman *et al.* in terms of statistical weight arguments. Oxygen with two unpaired electrons can have a final state with spin 3/2 or 1/2 after emission of the 1s electron. This gives a statistical weight of 4:2. The NO molecule has one unpaired electron, so the lines should have an intensity ratio of 3:1, in agreement with observation.

6) Electronic structure of metals.

X-ray photoelectron spectroscopy can in principle provide a direct determination if N(E), the density of states near the Fermi level. This subject has also been investigated with UV-photoelectron spectroscopy.

Fadley and Shirley[14] have studied the spectra of metallic iron, cobalt, nickel, copper, and platinum, and Fig. 18 shows some of their results. It can be seen from the figure that discrepancies exist between the x-ray and UV-photoelectron results, and that the x-ray results correspond more closely to the theoretically calculated electron distributions. A problem with UV-photoelectron spectroscopy may be that the 21 eV radiation which has been used is not of sufficient energy to eject the photoelectrons far enough into the continuum so that the final states are free from the effects of discrete levels lying just above the Fermi level and/or from plasmon oscillations. This problem was mentioned also in connection with x-ray absorption spectroscopy.

7) Catalysis.

The sensitivity of the photoelectron spectrum to surface conditions in solids has been noted. This suggests the possibility of applying the method to the study of catalysis.

Consider the thickness of the surface layer that is examined by the photoelectron method. Figure 19, from Siegbahn et al.,[1] shows the sensitivity of the technique to monolayer coverages of surfaces. The total amount of iodine in the sample was 10^{-8} gm and each double layer was 40 Å thick. From the saturation of peak area as a function of the film thickness, an estimate of 100 Å was made for the average depth of the emitted electrons in this material (mostly carbon). This is deeper than what is normally considered "surface", but nonetheless even the sub-surface properties of a catalyst may be of importance. Identification of oxidation states present in an activated catalyst may allow correlations with catalytic activity and ultimately optimization of catalyst performance. Elucidation of catalyst aging processes may also be possible. It may be feasible to do studies of particle size, since particles whose size are equal to or smaller than the penetration depth will be heavily weighted, giving an enhancement of lines from the small particles.

Figure 20 shows some portions of the photoelectron spectra taken of a catalytic material, FeV_2O_4, which was used for the dehydrogenation of cyclohexane.[15] One notes that, following the chemical reaction, the oxygen lines of the catalyst have shifted toward lower binding energy (more negative), the vanadium lines have shifted toward higher binding energy (more positive), and the Fe 3p line showed no shift. While these results are not yet well understood, it appears that there has been some electron transfer from vanadium to oxygen in the reaction.

8) Biochemistry.

Photoelectron spectroscopy may be quite useful in biochemical studies as an aid in understanding the role of certain widely-occurring elements such as iron and sulfur in molecules of biochemical significance. A study is being made by Kramer and Klein[16] of the binding energies of these elements in a variety of compounds with the hope of gaining information about the structures of their sites in iron-sulfur proteins. Some preliminary results are shown in Fig. 21, which demonstrates the large range in binding energy that is observable in these important compounds.

REFERENCES

*Work performed under the auspices of the U. S. Atomic Energy Commission.

1. Siegbahn, Nordling, Fahlman, Nordberg, Hamrin, Hedman, Johansson, Bergmark, Karlsson, Lindgren, and Lindberg, ESCA - Atomic, Molecular, and Solid State Structure Studied by Means of Electron Spectroscopy, (Almqvist and Wiksells, Uppsala, 1967).
2. T. Novakov and J. M. Hollander, unpublished results.
3. C. S. Fadley, S. B. M. Hagström, J. M. Hollander, M. P. Klein, and D. A. Shirley, Science 157, 1571 (1967); C. S. Fadley, S. B. M. Hagström, M. P. Klein, and D. A. Shirley, J. Chem. Phys. 48, 3779 (1968).
4. J. M. Hollander, D. N. Hendrickson, and W. L. Jolly, J. Chem. Phys. 49, 3315 (1968); D. N. Hendrickson, J. M. Hollander, and W. L. Jolly, Lawrence Radiation Laboratory Report UCRL-19027, July 1969, (J. Am. Chem. Soc., in press).
5. W. L. Jolly and D. N. Hendrickson, Lawrence Radiation Laboratory Report UCRL-19050, July 1969, (J. Am. Chem. Soc., in press).
6. L. G. Parratt, Rev. Mod. Phys. 31, 616 (1959).
7. T. Novakov and J. M. Hollander, Phys. Letters 13, 301 (1964).
8. T. Novakov and J. M. Hollander, Phys. Rev. Letters 21, 1133 (1969).
9. T. Novakov and J. M. Hollander, Bull. Am. Phys. Soc. 14, 524 (BM4) (1969).
10. M. O. Faltens, (Ph.D. Thesis) Lawrence Radiation Laboratory Report UCRL-18706, 1969.
11. R. E. Watson and A. J. Freeman, Hyperfine Interactions, ed. by A. J. Freeman and R. B. Frankel, (Academic Press, Inc., New York, 1967) p. 59 ff.
12. C. S. Fadley and D. A. Shirley, Lawrence Radiation Laboratory Report UCRL-18970, August 1969.

13. Hedman, Hedin, Nordling, and Siegbahn, private communication, June 1969.

14. C. S. Fadley and D. A. Shirley, Phys. Rev. Letters 21, 980 (1968).

15. W. N. Delgass, unpublished results, July 1969.

16. L. Kramer and M. P. Klein, unpublished results, June 1969.

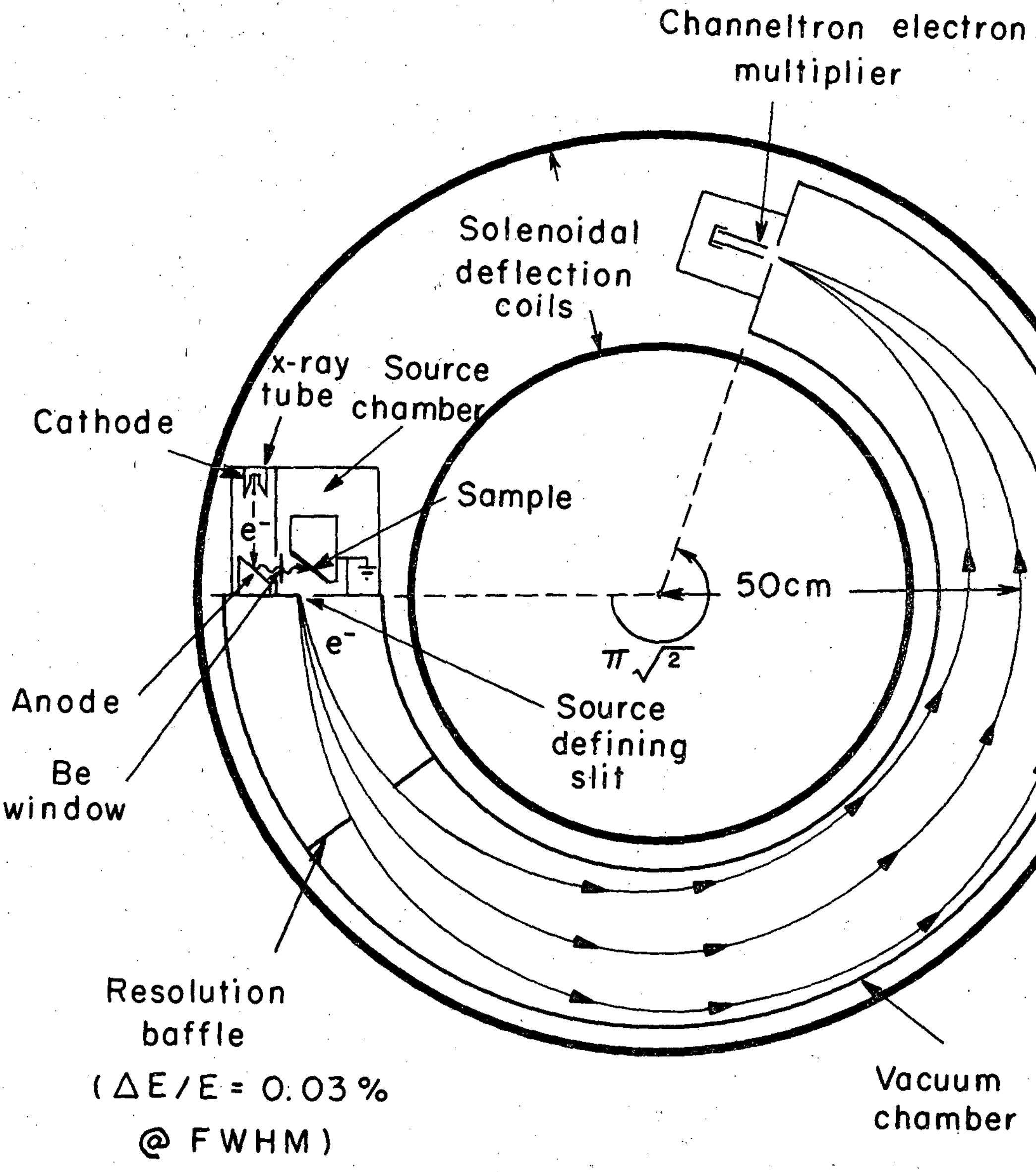

XBL694-2402

Fig. 1

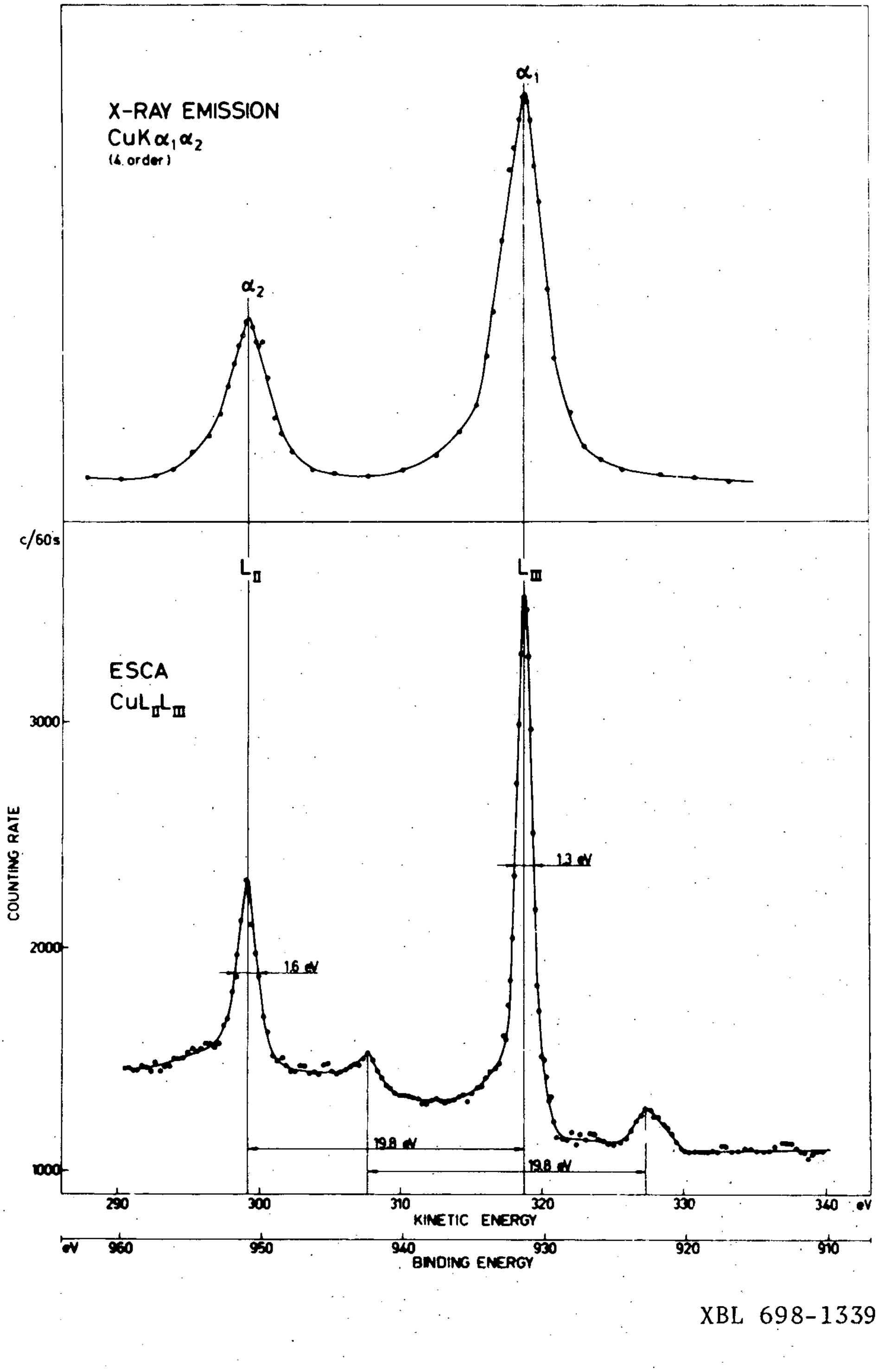

XBL 698-1339

Fig. 2

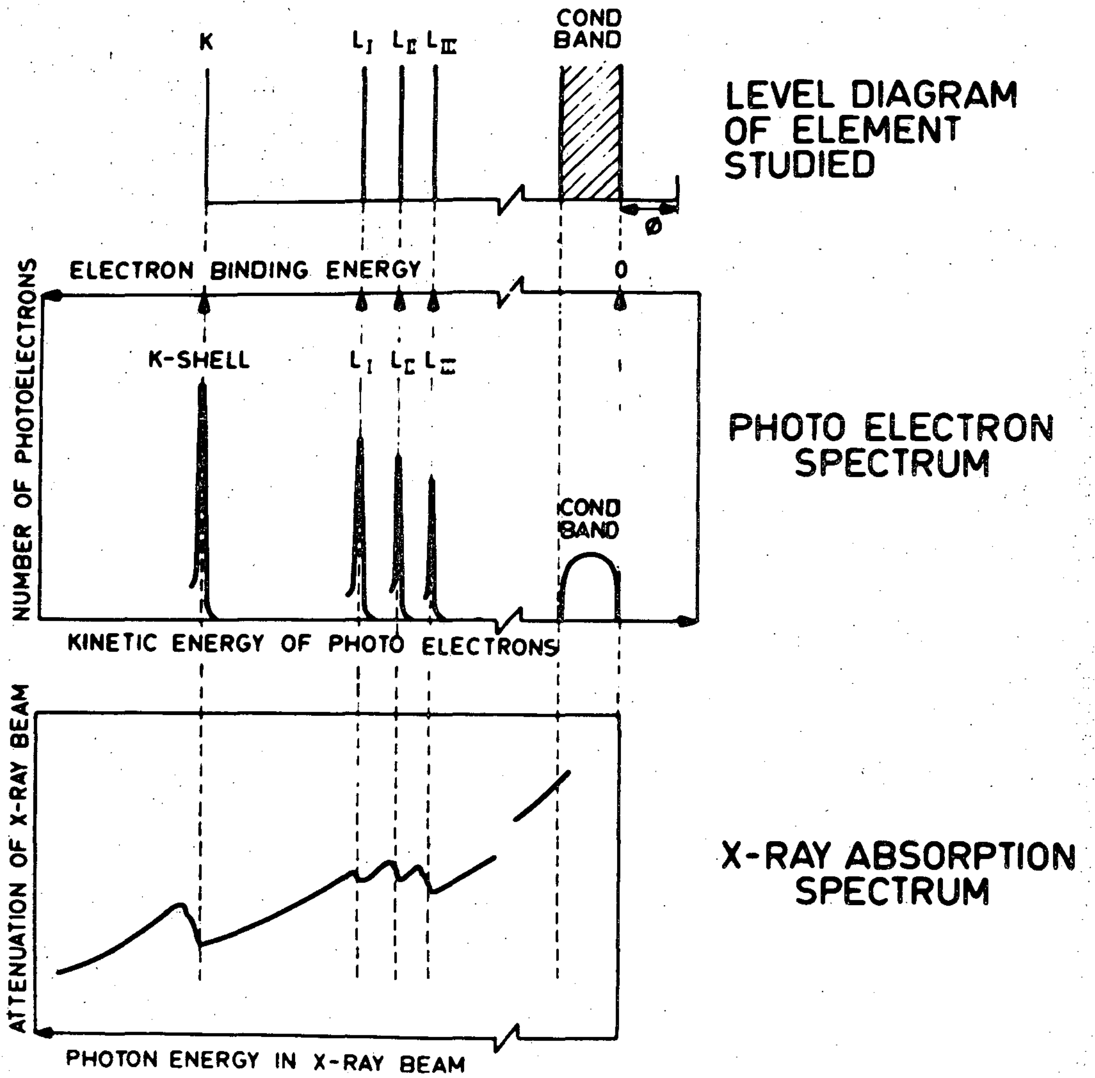

XBL 698-1341

Fig. 3

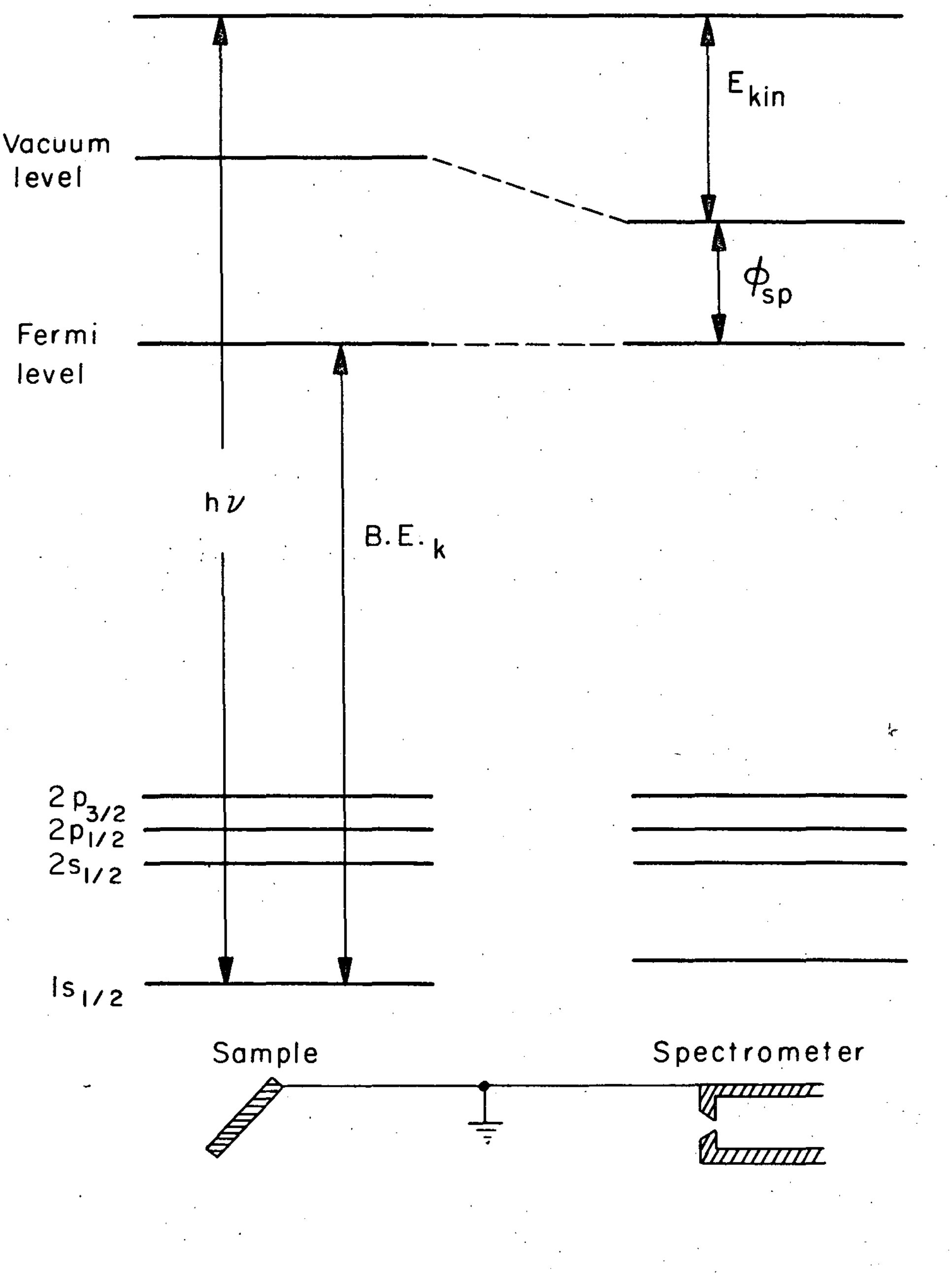

XBL698-3615

Fig. 4

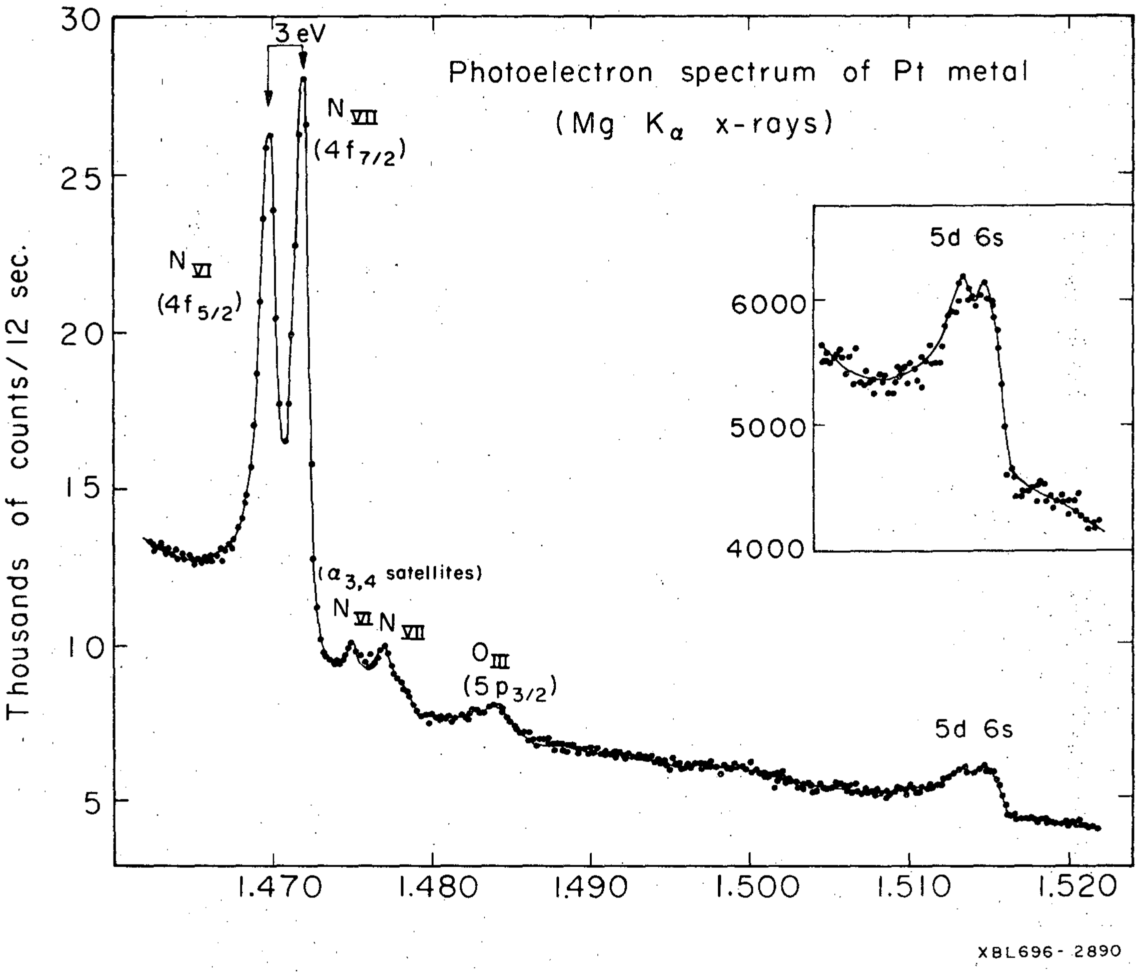
Photoelectron spectrum of Pt metal
(Mg K_α x-rays)
3 eV
N_{VII} ($4f_{7/2}$)
N_{VI} ($4f_{5/2}$)
($\alpha_{3,4}$ satellites)
N_{VI} N_{VII}
O_{III} ($5p_{3/2}$)
5d 6s
5d 6s
6000
5000
4000
Thousands of counts/12 sec.
30
25
20
15
10
5
1.470
1.480
1.490
1.500
1.510
1.520
XBL696-2890

Fig. 5

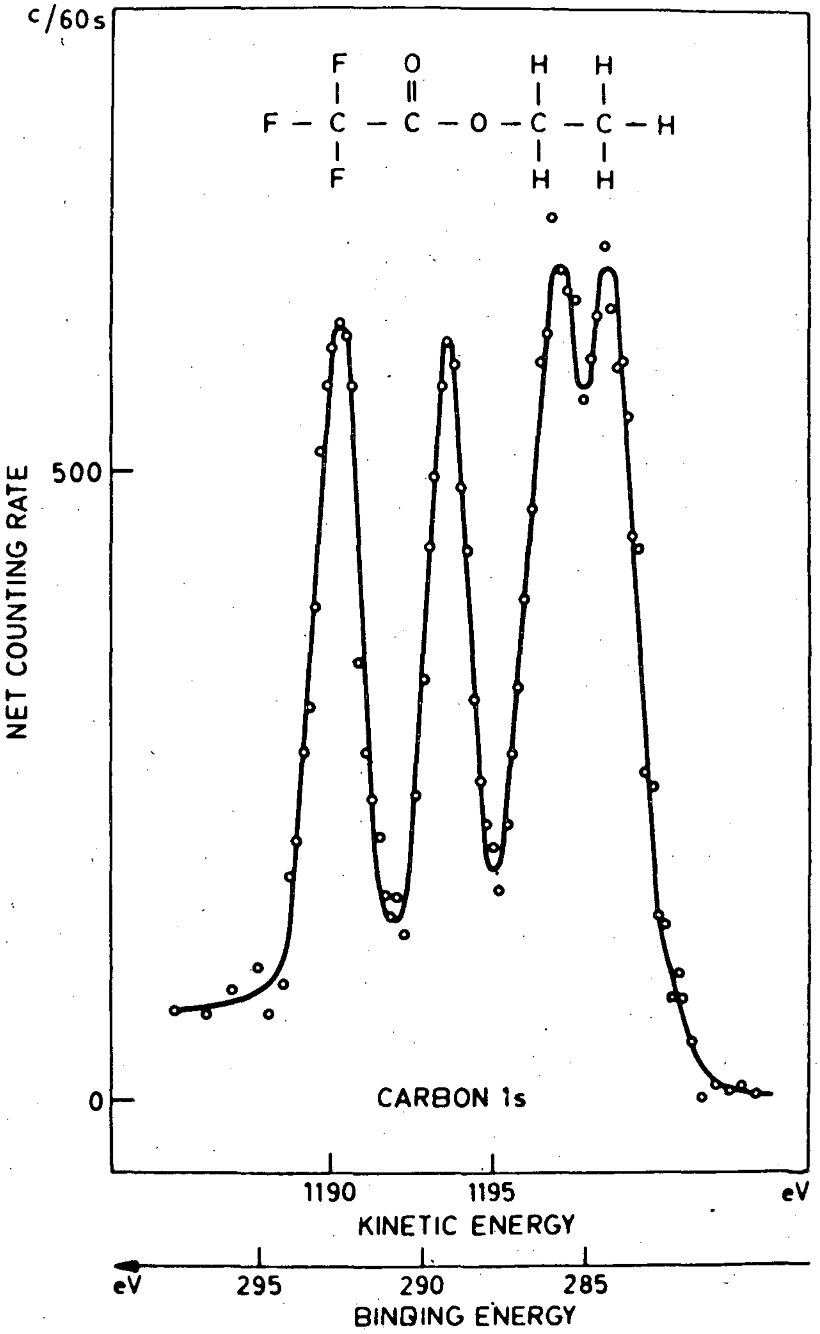

XBL 698-1340

Fig. 6

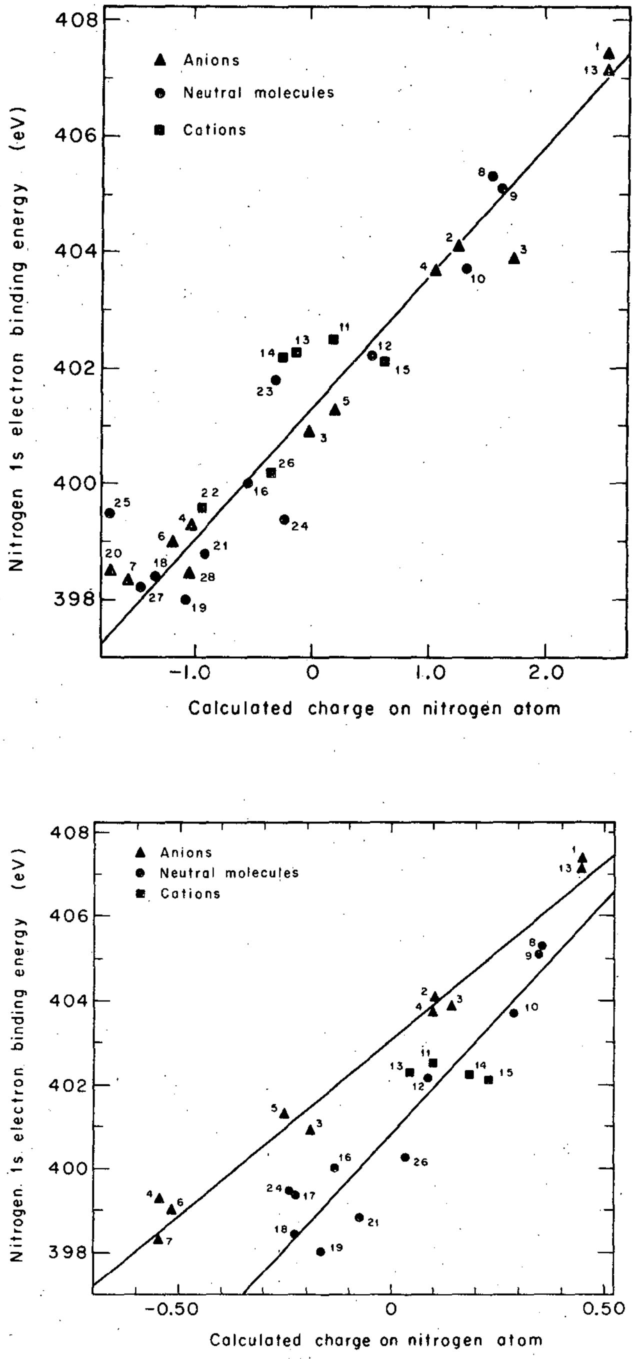

XBL 698-1347

Fig. 7

NITROGEN:

$$\mathrm{NaNO_2(s) + O^+(g) + O_3(g) \rightarrow 2O_3(s) + N^{+*}(g) + Na^+(g) + e^-(g)}$$

$$\mathrm{NaN_3(s) + O^+(g) + N_2O(g) \rightarrow 2N_2O(s) + N^{+*}(g) + Na^+(g) + e^-(g)}$$

$$\mathrm{KOCN(s) + O^+(g) + CO_2(g) \rightarrow 2CO_2(s) + N^{+*}(g) + K^+(g) + e^-(g)}$$

$$\mathrm{KCN(s) + O^+(g) + CO(g) \rightarrow 2CO(s) + N^{+*}(g) + K^+(g) + e^-(g)}$$

$$\mathrm{KSCN(s) + O^+(g) + SCO(g) \rightarrow 2SCO(s) + N^{+*}(g) + K^+(g) + e^-(g)}$$

CARBON:

$$\mathrm{CH_4(g) + N^+(g) \rightarrow NH_4{}^+(g) + C^{+*}(g) + e^-(g)}$$

$$\mathrm{NaHCO_3(s) + N^+(g) + HNO_3(g) \rightarrow Na^+(g) + 2HNO_3(s) + C^{+*}(g) + e^-(g)}$$

$$\mathrm{NaCH_3CO_2(s) + N^+(g) + CH_3NO_2(g) \rightarrow Na^+(g) + 2CH_3NO_2(s) + C^{+*}(g) + e^-(g)}$$

$$\mathrm{KCN(s) + N^+(g) + N_2(g) \rightarrow K^+(g) + 2N_2(s) + C^{+*}(g) + e^-(g)}$$

$$\mathrm{CO_2(g) + N^+(g) \rightarrow NO_2{}^+ + C^{+*}(g) + e^-(g)}$$

BORON:

$$\mathrm{NaBH_4(s) + C^+(g) + CH_4(g) \rightarrow Na^+(g) + 2CH_4(s) + B^{+*}(g) + e^-(g)}$$

$$\mathrm{NaBF_4(s) + C^+(g) + CF_4(g) \rightarrow Na^+(g) + 2CF_4(s) + B^{+*}(g) + e^-(g)}$$

IODINE:

$$\mathrm{KI(s) + Xe^+(g) + Xe(g) \rightarrow K^+(g) + 2Xe(s) + I^{+*}(g) + e^-(g)}$$

$$\mathrm{KIO_3(s) + Xe^+(g) + XeO_3(g) \rightarrow K^+(g) + 2XeO_3(s) + I^{+*}(g) + e^-(g)}$$

$$\mathrm{KIO_4(s) + Xe^+(g) + XeO_4(g) \rightarrow K^+(g) + 2XeO_4(s) + I^{+*}(g) + e^-(g)}$$

XBL 698-1344

Fig. 8

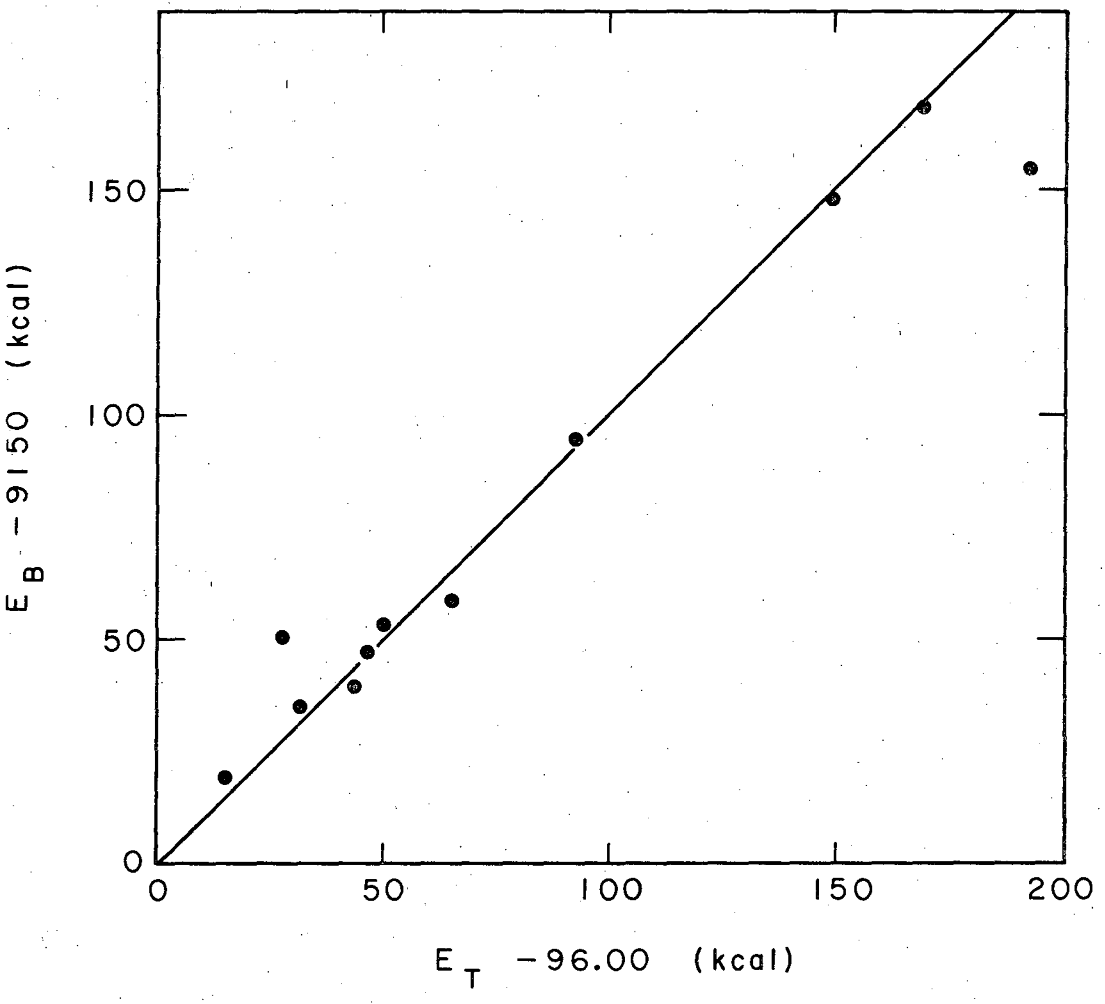

XBL695-2747

Fig. 9

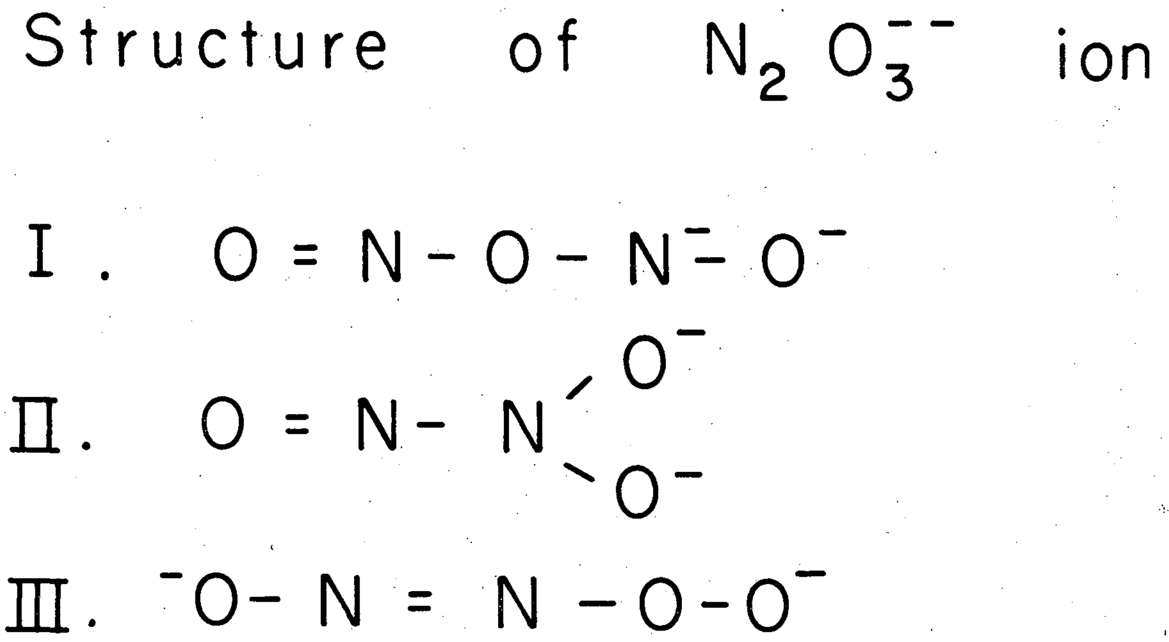

XBL696-2891

Fig. 10

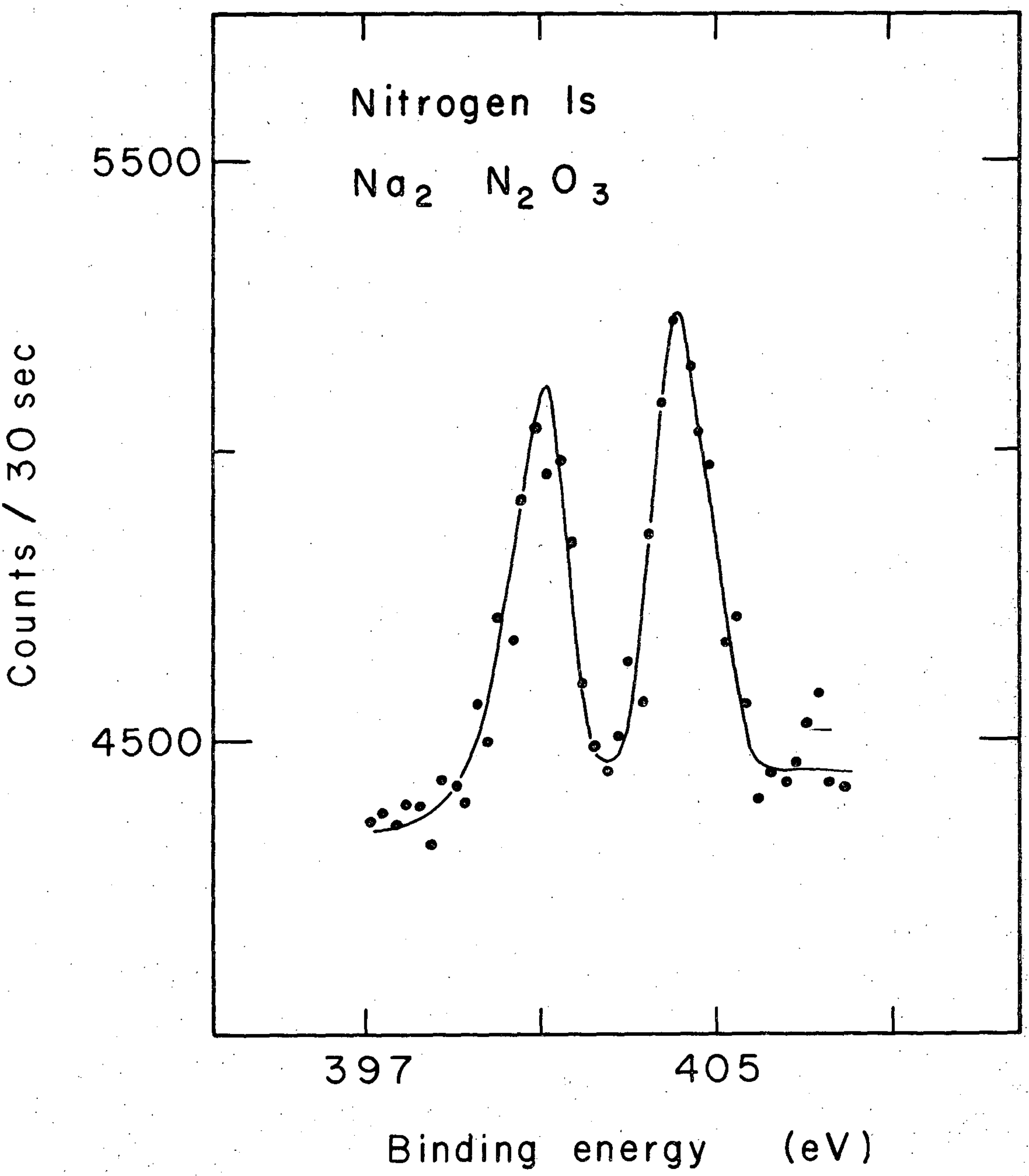

XBL 696-2976

Fig. 11

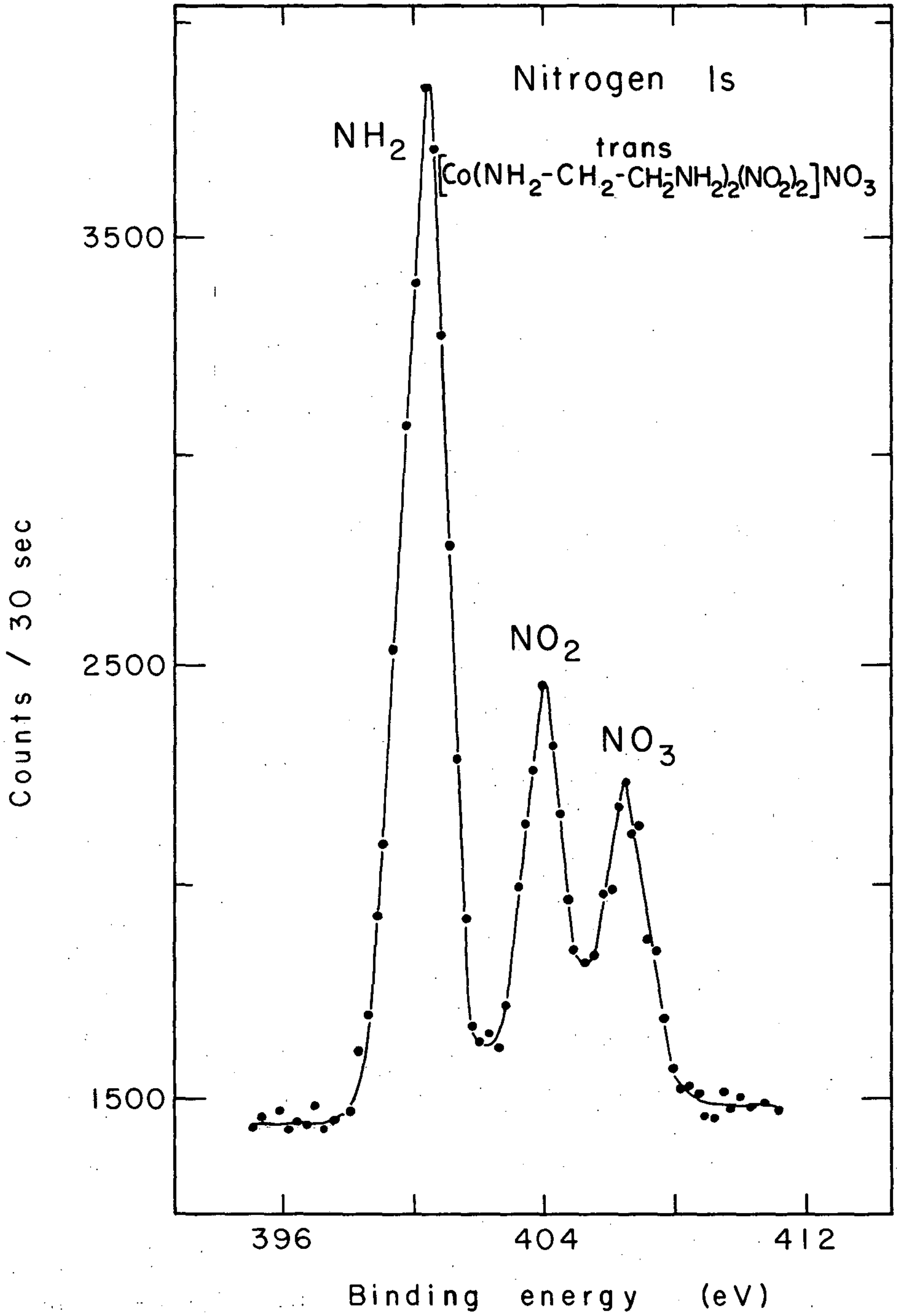

XBL 696-2975

Fig. 12

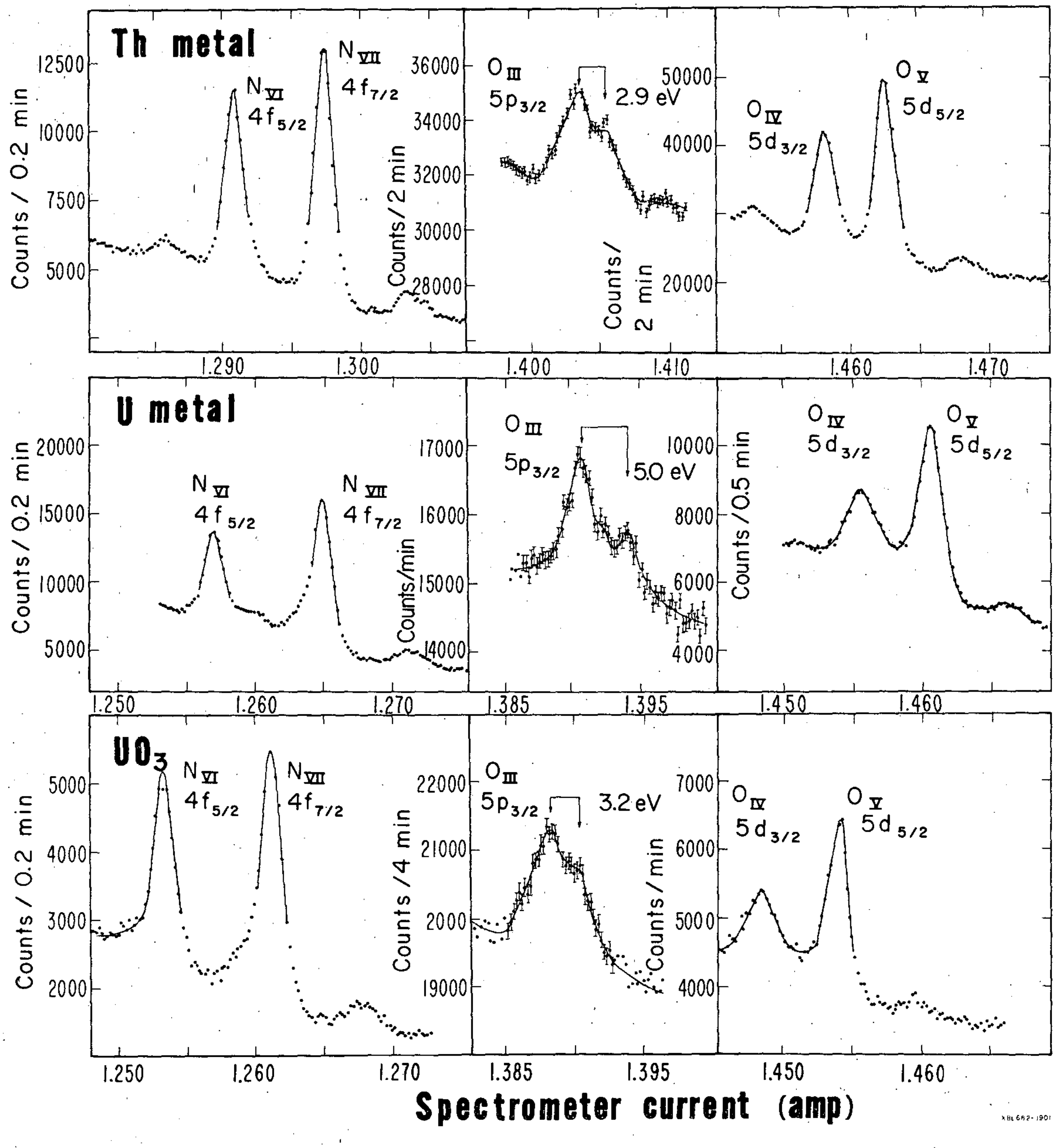
Th metal
U metal
UO_3
N_{VI} $4f_{5/2}$
N_{VII} $4f_{7/2}$
O_{III} $5p_{3/2}$
2.9 eV
5.0 eV
3.2 eV
O_{IV} $5d_{3/2}$
O_{V} $5d_{5/2}$
Counts / 0.2 min
Counts/2 min
Counts/min
Counts /0.5 min
Counts /4 min
Counts / min
12500
10000
7500
5000
36000
34000
32000
30000
28000
50000
40000
20000
20000
15000
17000
16000
15000
14000
10000
8000
6000
4000
5000
4000
3000
2000
22000
21000
2000
19000
7000
6000
5000
1.290
1.300
1.400
1.410
1.460
1.470
1.250
1.260
1.270
1.385
1.395
1.450
Spectrometer current (amp)
XBL 692-1901

Fig. 13

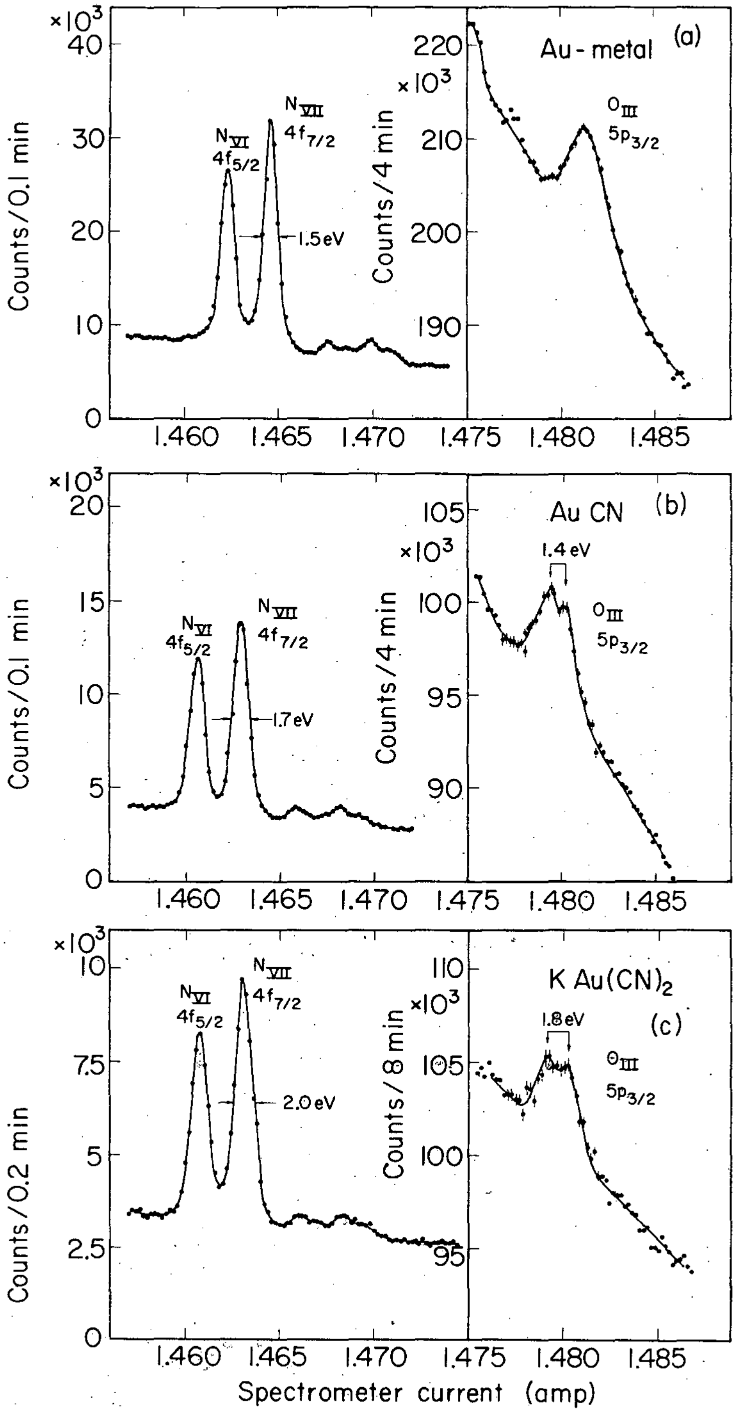

XBL694-2338

Fig. 14

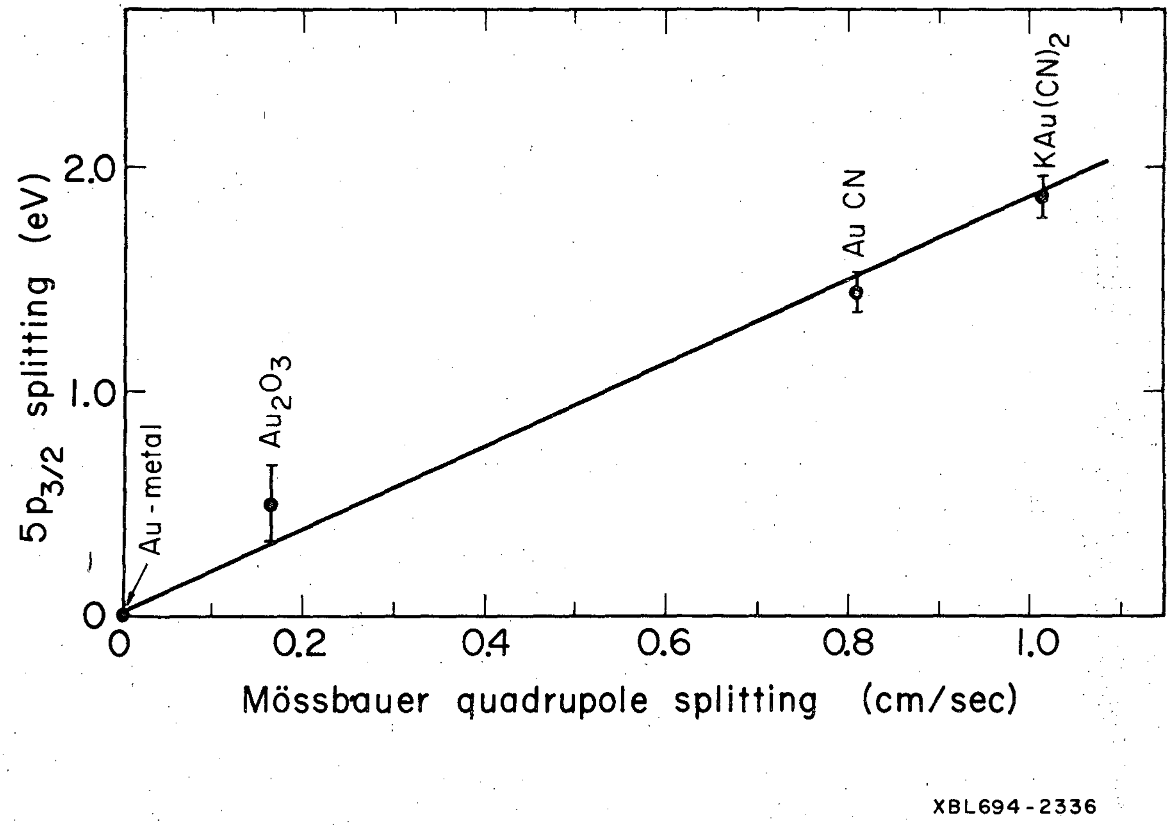
5p3/2 splitting (eV)
0
1.0
2.0
Au-metal
Au2O3
Au CN
KAu(CN)2
0
0.2
0.4
0.6
0.8
1.0
Mössbauer quadrupole splitting (cm/sec)
XBL694-2336

Fig. 15

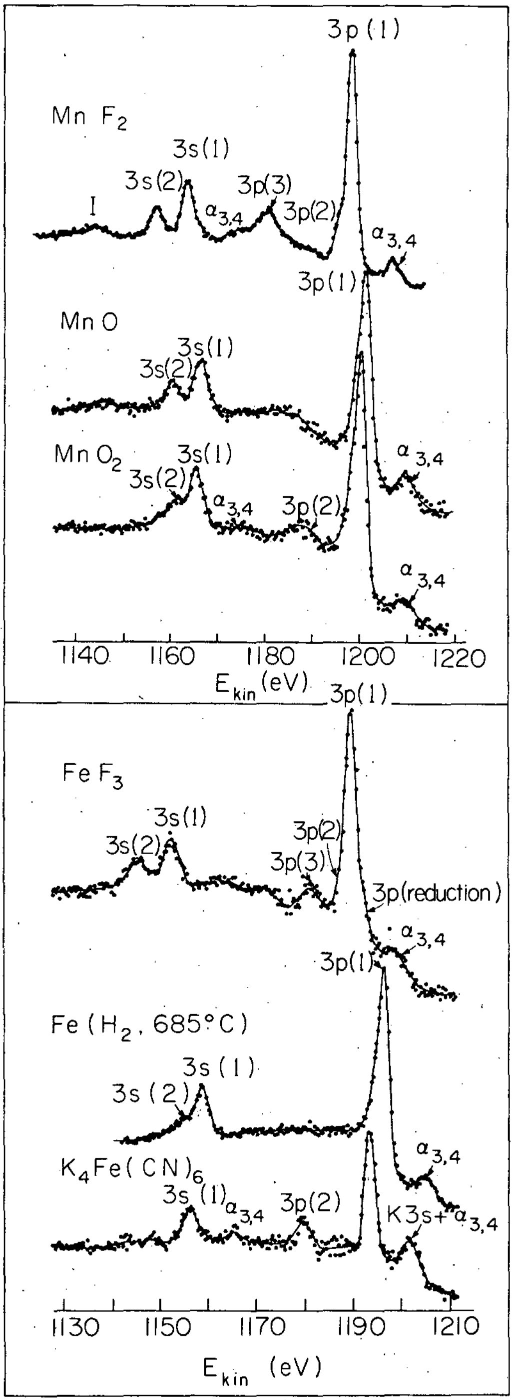

XBL698-3635

Fig. 16

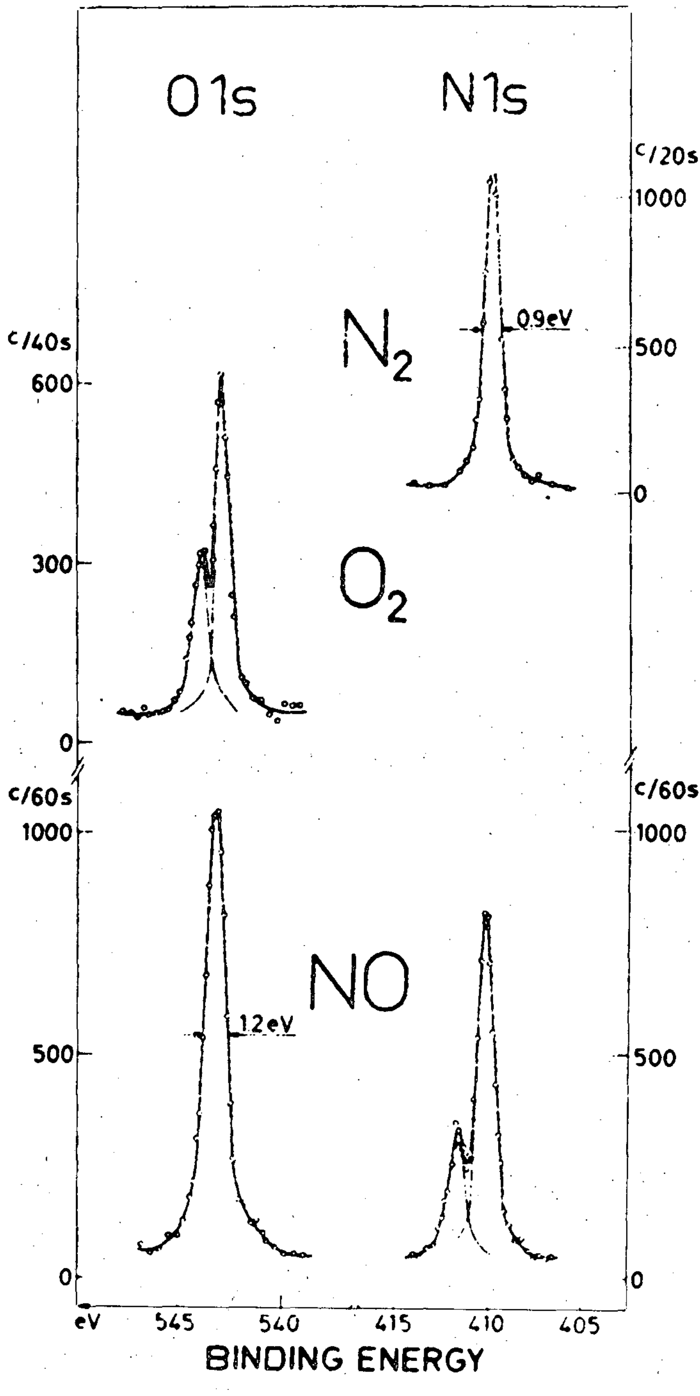

XBL 698-1342

Fig. 17

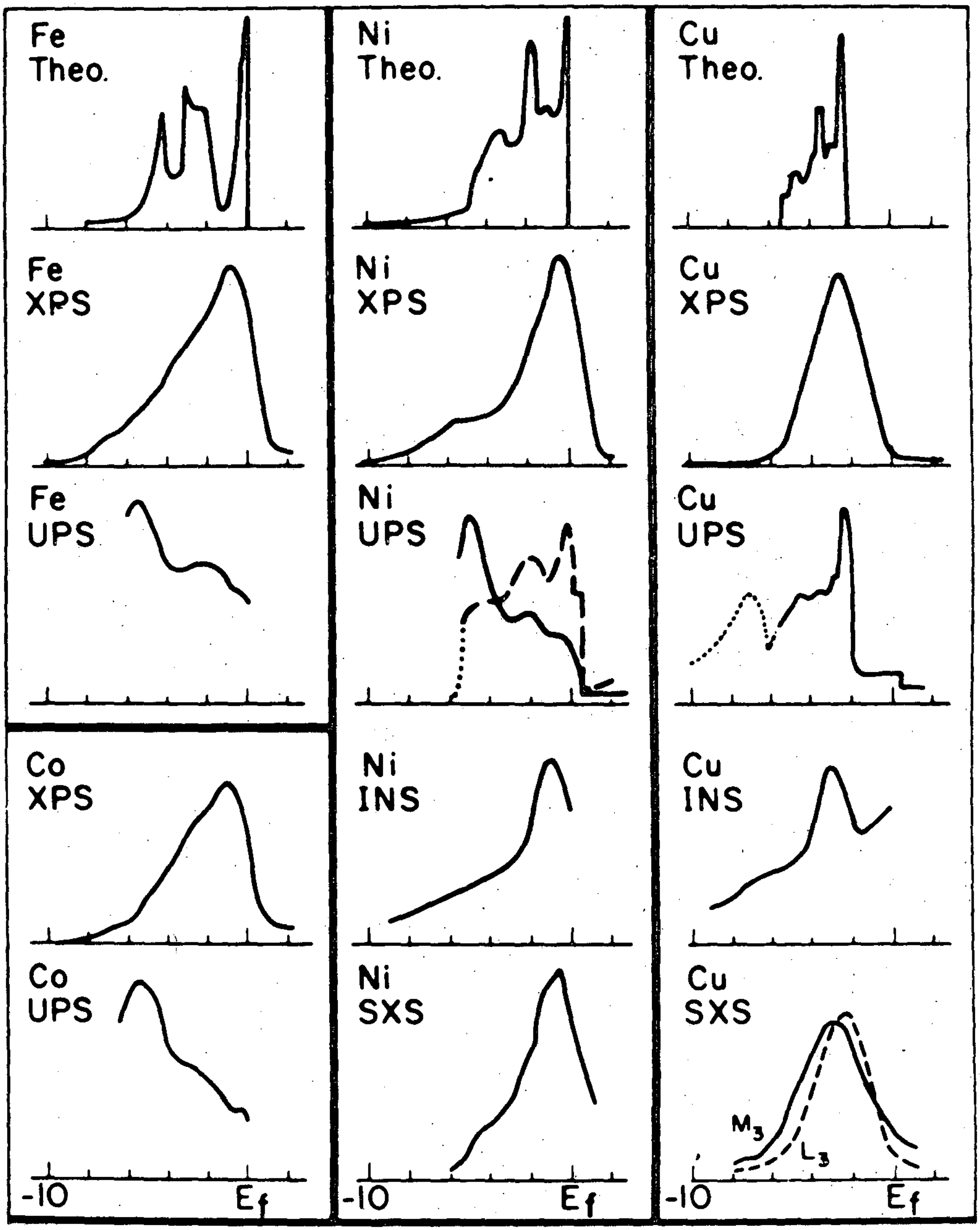

XBL 698-1345

Fig. 18

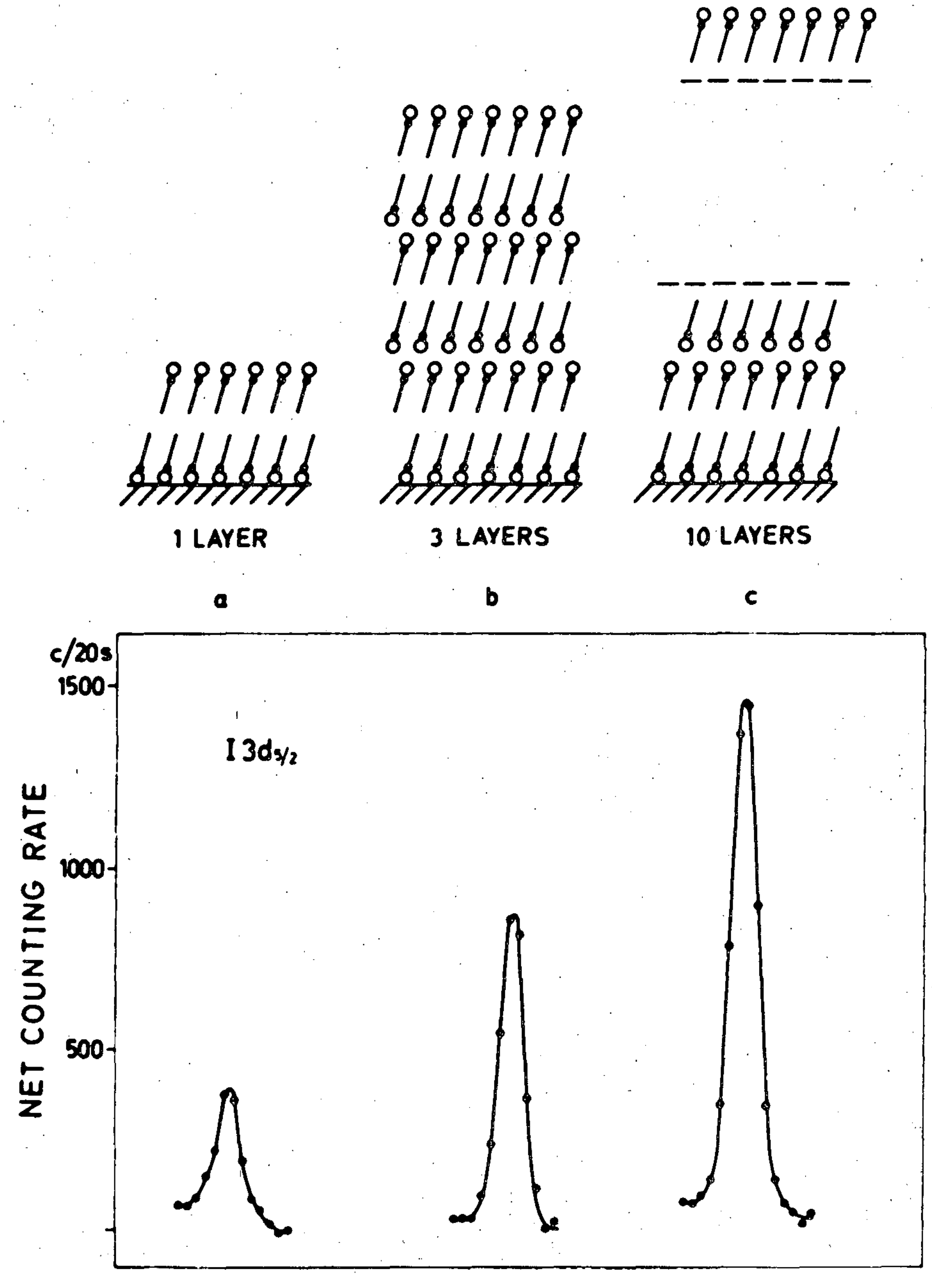

XBL 698-1343

Fig. 19

Fig. 20

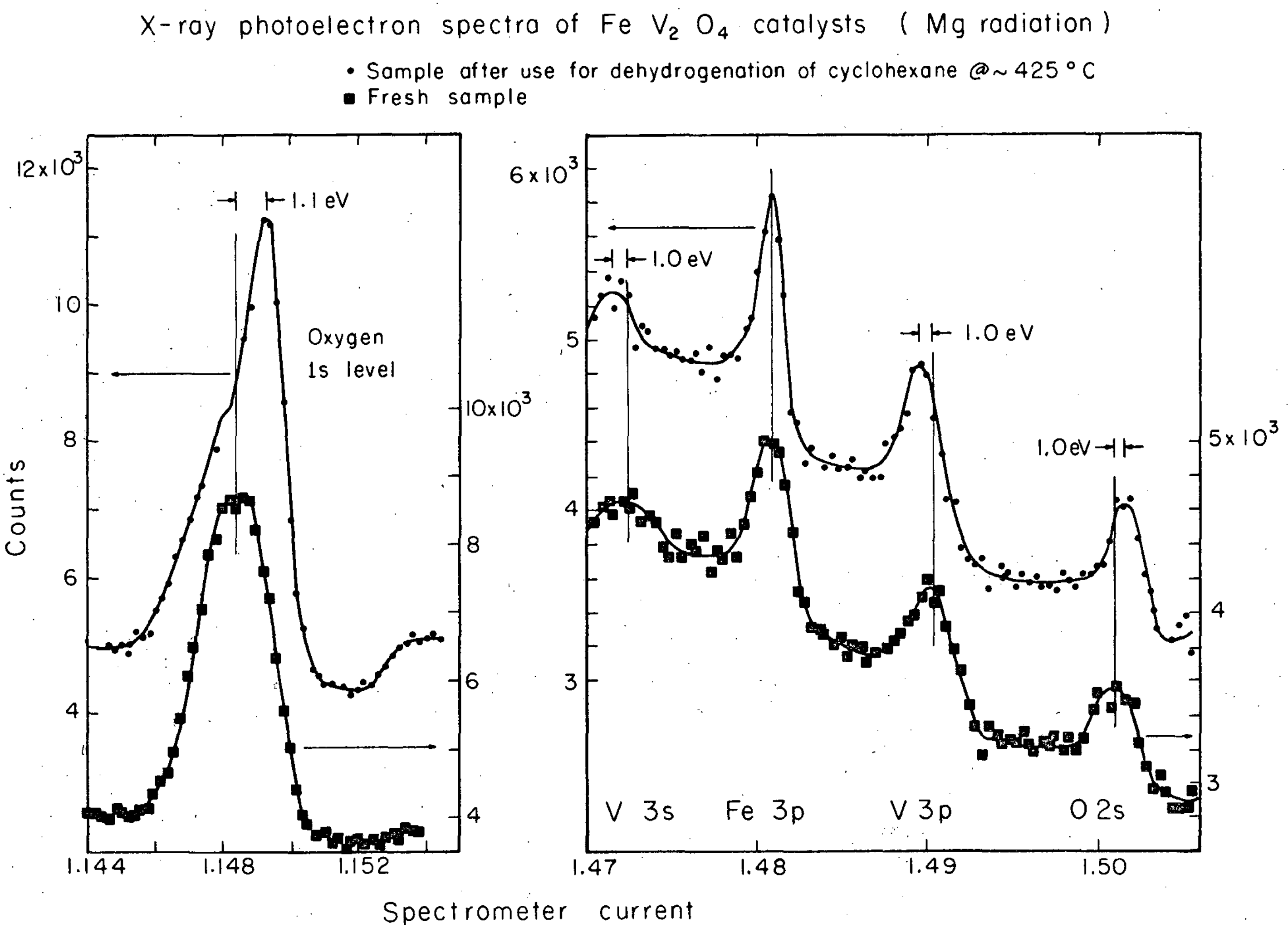

X-ray photoelectron spectra of Fe V_2 O_4 catalysts (Mg radiation)

XBL694-2487

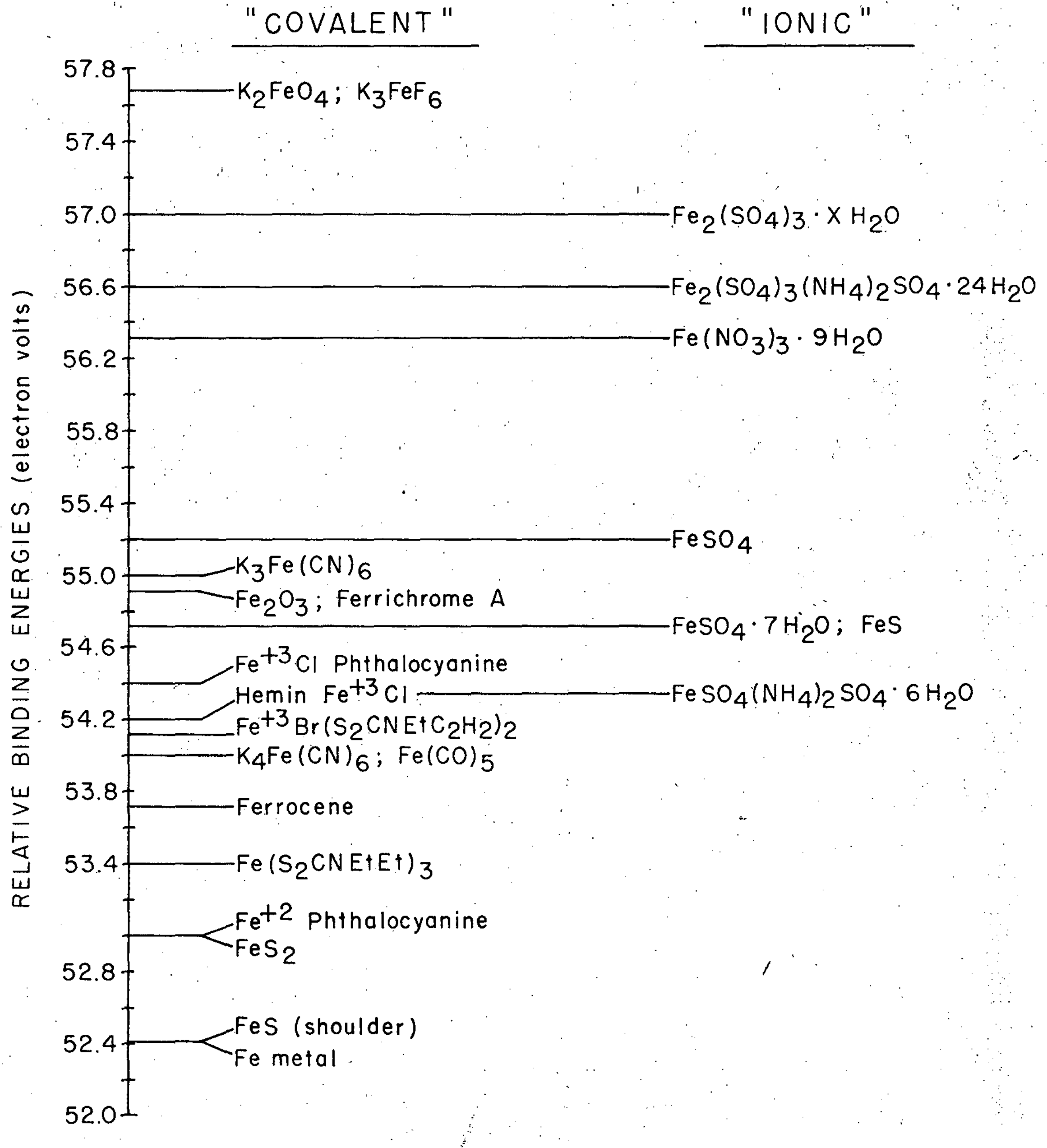
"COVALENT"
"IONIC"
RELATIVE BINDING ENERGIES (electron volts)
57.8
57.4
57.0
56.6
56.2
55.8
55.4
55.0
54.6
54.2
53.8
53.4
52.8
52.4
52.0
K2FeO4; K3FeF6
Fe2(SO4)3 · X H2O
Fe2(SO4)3(NH4)2SO4 · 24H2O
Fe(NO3)3 · 9H2O
FeSO4
K3Fe(CN)6
Fe2O3; Ferrichrome A
FeSO4 · 7H2O; FeS
Fe+3Cl Phthalocyanine
Hemin Fe+3Cl
FeSO4(NH4)2SO4 · 6H2O
Fe+3Br(S2CNEtC2H2)2
K4Fe(CN)6; Fe(CO)5
Ferrocene
Fe(S2CNEtEt)3
Fe+2 Phthalocyanine
FeS2
FeS (shoulder)
Fe metal
XBL695-4274

Fig. 21

TECHNICAL INFORMATION DIVISION
LAWRENCE RADIATION LABORATORY
UNIVERSITY OF CALIFORNIA
BERKELEY, CALIFORNIA 94720